Materials Characterization xxx (xxxx) 112580

Contents lists available at ScienceDirect

Materials Characterization

journal homepage: www.elsevier.com/locate/matchar

Effect of aging temperature on the hardening behavior and precipitation evolution of Mg—10Gd alloy

Kang Wei [a, b], Lirong Xiao [a], Bo Gao [a], Qingzhong Mao [a], Yi Liu [a], Lei Li [a], Wenwen Sun [c], Yudong Sui [d], Hao Zhou [a, *], Yonghao Zhao [a, *]

[a] Nano and Heterogeneous Materials Center, School of Materials Science and Engineering, Nanjing University of Science and Technology, Nanjing 210094, China
[b] Jiangxi Key Laboratory of Forming and Joining Technology for Aviation Components, Nanchang Hangkong University, Nanchang 330063, China
[c] Department of Materials Science and Engineering, Southeast University, Nanjing 211189, China
[d] School of Materials Science and Engineering, Kunming University of Science and Technology, Kunming 650093, China

ARTICLE INFO

Keywords:
Mg—Gd alloy
Aging temperature
Hardening behavior
Precipitate
HAADF-STEM

ABSTRACT

Mg alloys containing high Gd are featured by the outstanding aging hardening response. Here we conduct a systematic study on the hardening behavior and precipitation evolution in a Mg—10Gd alloy during isothermal aging at 200–250 °C by atomic-resolution high-angle annular dark-field scanning transmission electron microscopy (HAADF-STEM). The optimum aging temperature of Mg—10Gd is 200 °C with peak hardness of 102.4 HV. Hardness improvement of the aged samples at 200 °C mainly originates from precipitation strengthening, and β' nano-precipitates with fine size of 10 nm are the main strengthening phases. The samples exhibit a certain aging hardening effect at 225 °C with peak hardness of 89.4 HV, due to the gourd-shaped β' precipitates with coarse size of 100 nm. Furthermore, various metastable nanoscale structures (including short-range ordered GP zones, β'', β_T, β_M and β_F' phases) are observed in the aged samples, and their formation mechanisms are rationalized in detail.

1. Introduction

With energy conservation and environmental protection formally proposed in recent years, magnesium (Mg) and its alloys are considered as the lightest promising structural materials for potential applications in aerospace, automotive and biomedical industries [1–3]. However, compared with other metallic materials such as steels, aluminum alloys and titanium alloys, Mg alloys exhibit the lower strength at room and high temperature [4–6]. To date, it has been widely proven that precipitation hardening is an effective and convenient approach to improve the strength of various Mg alloys, including the prototypical Mg—Al, Mg—Zn and Mg-rare earth (RE) based alloys [7–9]. Gd is a common RE element that offers Mg alloys with the strong aging hardening effect. The mechanical properties are closely related to the type, size and spacing of nanoscale precipitates in Mg—Gd alloys [10–12].

The aging precipitation kinetics of Mg—Gd alloys has been intensively studied using both computational and experimental tools, and its affecting factors (including Gd content, deformation amount, grain size, etc.) have been reported in previous literatures [13–19]. Zhang et al. [9] and Li et al. [14] found that Mg alloys with Gd content of above 10 wt% exhibited a remarkable aging hardening response, which was largely attributed to the increased driving force of precipitates caused by high supersaturation of Gd element during the aging process. Čížek et al. [15] investigated the influence of deformation on precipitation process in Mg—15Gd alloy by transmission electron microscopy (TEM) combined with positron lifetime spectroscopy. Their results suggested that dislocations facilitated nucleation of precipitates, and the required optimum aging temperature was decreased with increasing deformation amount, leading to a higher peak hardness in cold rolled samples after aging treatment. Wan et al. [16] further reported that grain refinement was beneficial to enhancing the peak hardness and strength in the aged Mg-Gd-Y-Zr alloy. Meanwhile, the aging hardening responses in rolled Mg-14Gd-2Ag-0.5Zr alloys with different grain sizes were studied by Li et al. [17]. They found that compared with the coarse-grained sample with an average grain size ($\overline{d}$) of 20 μm, the significantly improved aging hardening response was obtained in the fine-grained sample ($\overline{d}$ = 3 μm) due to the segregation of solute atoms into the nano subgrain boundaries during aging process. Moreover, previous researches also revealed that aging temperature served as a key factor altering the precipitation behavior in Mg—Gd based alloys [20–23]. It was found

* Corresponding author.
E-mail addresses: hzhou511@njust.edu.cn (H. Zhou), yhzhao@njust.edu.cn (Y. Zhao).

https://doi.org/10.1016/j.matchar.2022.112580
Received 27 September 2022; Received in revised form 29 November 2022; Accepted 9 December 2022
1044-5803/

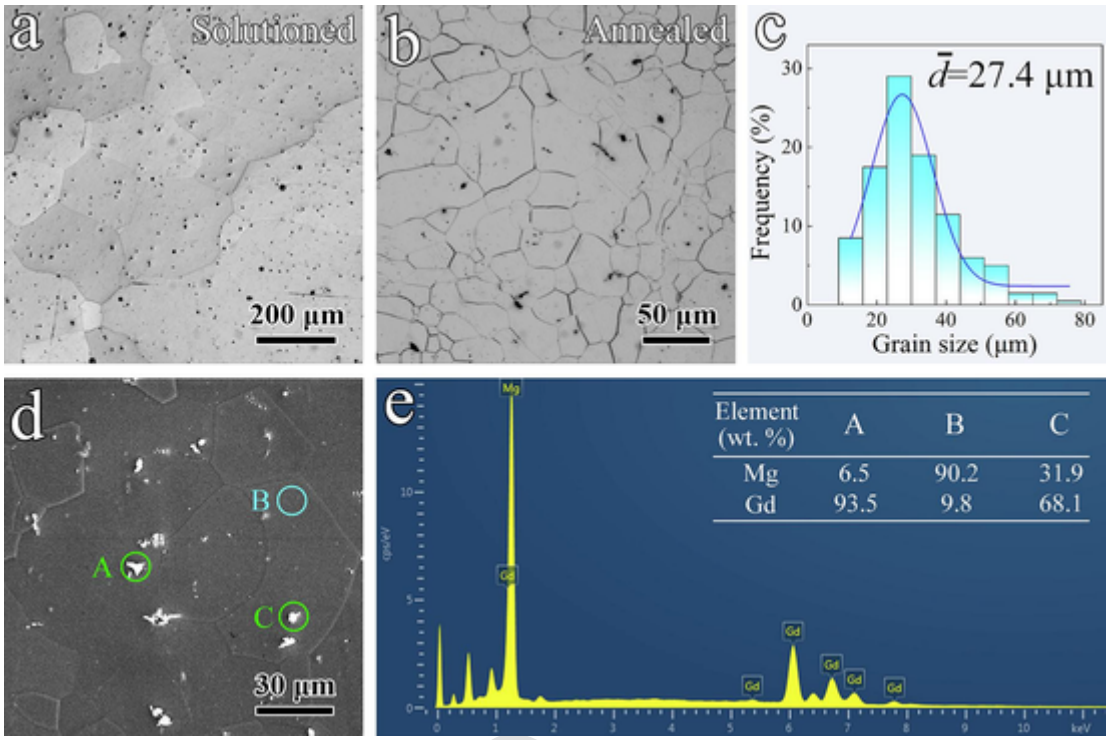

Fig. 1. Microstructure analysis of Mg—Gd alloy before aging treatment: (a) and (b) optical microstructure of solid solute and annealed samples, respectively; (c) grain size distribution of annealed sample; (d) SEM images showing annealed sample, and the eutectic compounds are marked by A and C green circles; (e) EDS spectrum with element contents. (For interpretation of the references to colour in this figure legend, the reader is referred to the web version of this article.)

that the time required to reach the peak hardness was reduced gradually with raising aging temperature, and ideal strengthening effects could be obtained in the samples aged at 200–250 °C. In addition, the precipitation sequences and some novel phases of Mg—Gd alloys have also been clarified in recent studies using Cs-corrected HAADF-STEM [24–28]. However, the effect of age temperature on the hardening response in Mg—Gd alloys still lacks systematic investigations, and the detailed precipitate features at atomic scale are not fully understood due to the limited resolution of traditional characterization methods.

In the present work, the hardening behavior and precipitation evolution in Mg—10Gd binary alloy aged at 200–250 °C for 5–80 h were comprehensively studied via advanced atomic-resolution HAADF-STEM. The age-hardening curves of Mg—10Gd samples were obtained. In addition, the atomic structures of precipitate phases as well as their formation mechanisms were analyzed and rationalized in detail. The findings obtained in this study contribute to rationally designing heat treatment process for the optimization of mechanical properties in Mg alloys with high RE content.

2. Experimental procedures

The Mg—10Gd (wt%) ingots were prepared by melting high purity Mg (99.99%) and Mg—25Gd (wt%) master alloys in an electric resistance furnace under a mixed protective atmosphere of CO_2 and SF_6 with the volume ratio of 100:1. The details of alloy preparation have been reported in our previous studies [29]. Then, the as-cast ingots were homogenized at 530 °C for 12 h followed by water quenching, and machined into sheets with thickness of 4.5 mm. Cold rolling was carried out from 4.5 mm to 3.6 mm thickness with a total reduction of ~20%. The rolled samples were annealed at 450 °C for 20 min with argon protection. The actual chemical composition of the studied alloys was Mg-9.8Gd (wt%), which was tested by an inductively coupled plasma (ICP, Plasma 3000) apparatus. The alloys are brief to Mg—Gd alloys for convenience in following.

Isothermal aging experiments were performed in an oil bath furnace at 200 °C, 225 °C and 250 °C for 5–80 h. Vickers microhardness was measured by a Shimadzu HMV-G hardness tester with a load of 980.7 mN and a dwell time of 15 s. Twenty indentations were tested to obtain reliable results for each sample. The microstructures of Mg—Gd samples before and after aging treatment were examined by an Olympus BX41M-LED optical microscope (OM). Samples for OM observations were ground with sandpapers of 320, 800, 1200 and 2000 grits, followed by mechanical polishing to mirror-like surfaces, and then etched by an ethanol solution with 5 vol% of nitric acid. Electron back scattering diffraction (EBSD) analysis was performed on a Zeiss Auriga scanning electron microscope (SEM) equipped with Channel 5 software. The accelerate voltage and scanning step size were set as 15 kV and 2 μm, respectively. EBSD specimen surfaces were mechanically polished and then electropolished in an electrolyte containing 97 vol% ethanol and 3 vol% perchloric acid at 20 V and − 30 °C for 120 s. HAADF-STEM and bright-field TEM observations were carried out using an aberration-corrected high-resolution transmission electron microscope (FEI Titan G2 60–300) operated at 300 kV. TEM foils were sliced from the aged samples by a Buehler Isomet low-speed saw and gently ground to a final thickness of ~25 μm, and then ion-milled to perforation at a Gatan PIPS 691 machine with a low beam energy (4 keV) and a low angle (5°).

3. Results and discussions

3.1. Microstructures of solutioned and annealed mg—Gd samples

Fig. 1a shows the microstructure of solid solute Mg—Gd sample, which exhibits a typical coarse-grained structure with grain size of 150–200 μm. After cold rolling and annealing treatment, significant microstructural refinement is obtained (Fig. 1b), which has an average grain size ($\bar{d}$) of ~27.4 μm (Fig. 1c). Meanwhile, some small block phases (marked by the green circles of A and C) are found in the annealed sample, which are residual eutectic compounds of incomplete

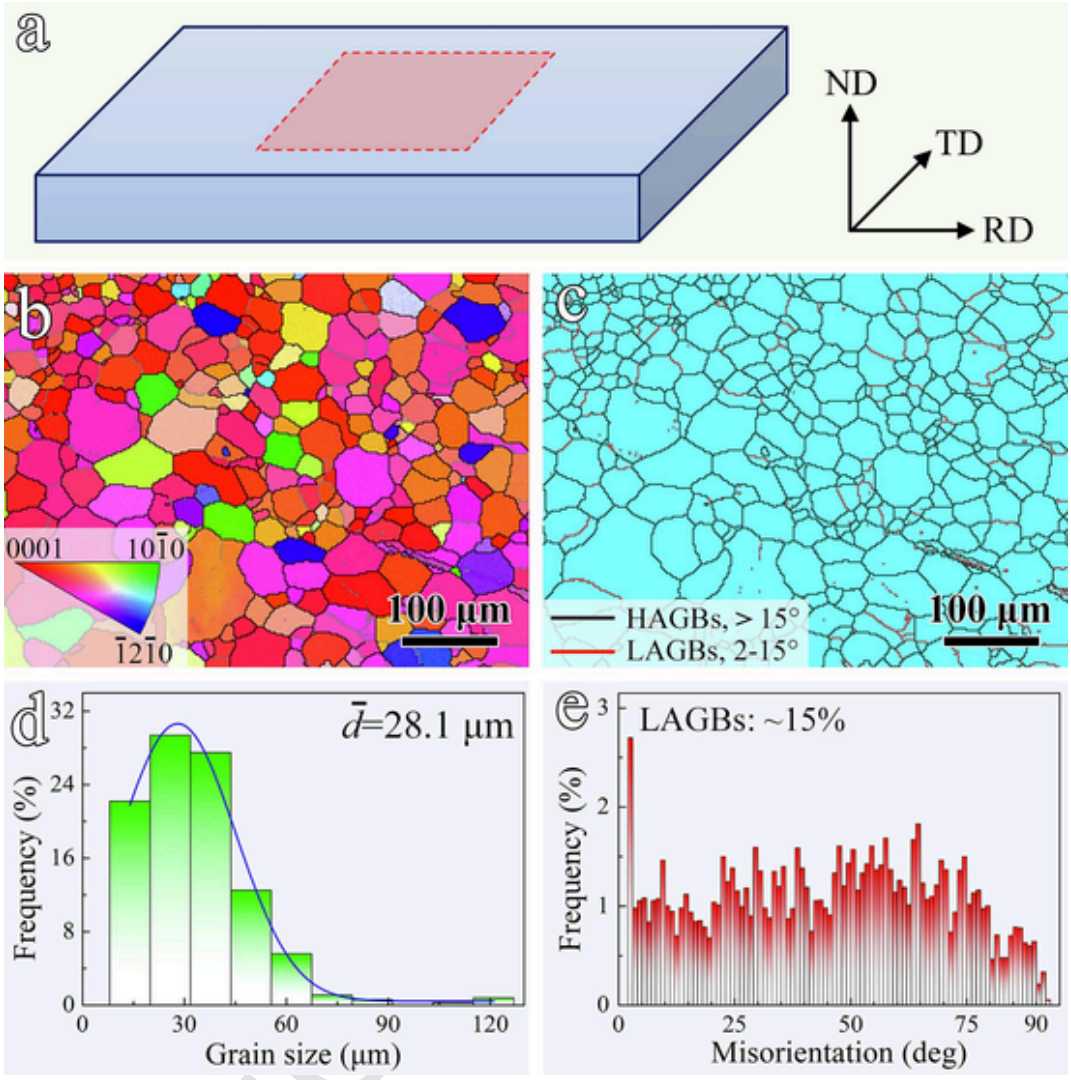

Fig. 2. EBSD micrographs of annealed Mg—Gd alloy: (a) sketch of the coordinate reference system of sample, EBSD micrograph is taken from the dash rectangle area; (b) inverse pole figure mapping; (c) HCP phase and grain boundary mapping; (d) grain size distribution; (e) grain boundary misorientation distribution.

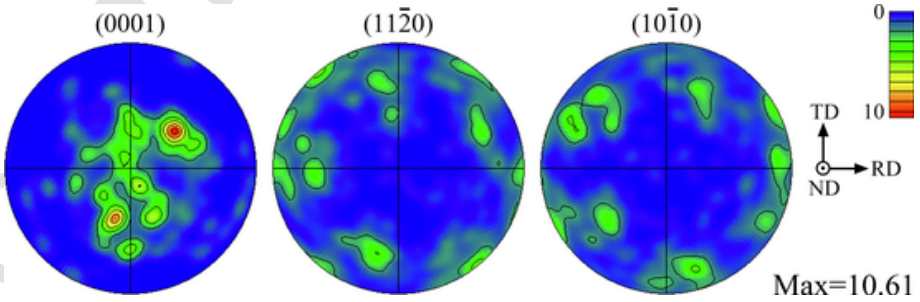

Fig. 3. Pole figures of (0001), $(11\bar{2}0)$ and $(10\bar{1}0)$ in Mg—Gd sample.

solid solution, as shown in Fig. 1d. Based on the corresponding EDS spectrum in Fig. 1e, these eutectic compounds are mainly rich in Gd element with mass fraction higher than 60%.

EBSD analysis was performed along the normal direction (ND) of the Mg—Gd rolling sheet, as shown in Fig. 2a. The annealed sample exhibits a uniform distributed grain structure (Fig. 2b), and its average grain size ($\bar{d}$) is ~28.1 μm (Fig. 2d). Meanwhile, Fig. 2c shows the distribution map of grain boundary, in which high angle grain boundaries (HAGBs, >15°) and low angle grain boundaries (LAGBs, 2–15°) are marked by black and red lines, respectively. The fraction of LAGBs is only ~15% (Fig. 2e), which also indicates that the dislocations were mostly recovered during the annealing process, achieving fully recrystallization after annealing.

Fig. 3 shows the pole figures of (0001), $(11\bar{2}0)$ and $(10\bar{1}0)$ of annealed sample. Clearly, (0001) pole figure is characterized by a typical bimodal texture with maximum intensity value of 10.61 mrd, and the angle between *c*-axis of grains and ND direction is ~39°, which showing a weak basal texture of Mg—Gd annealed plate.

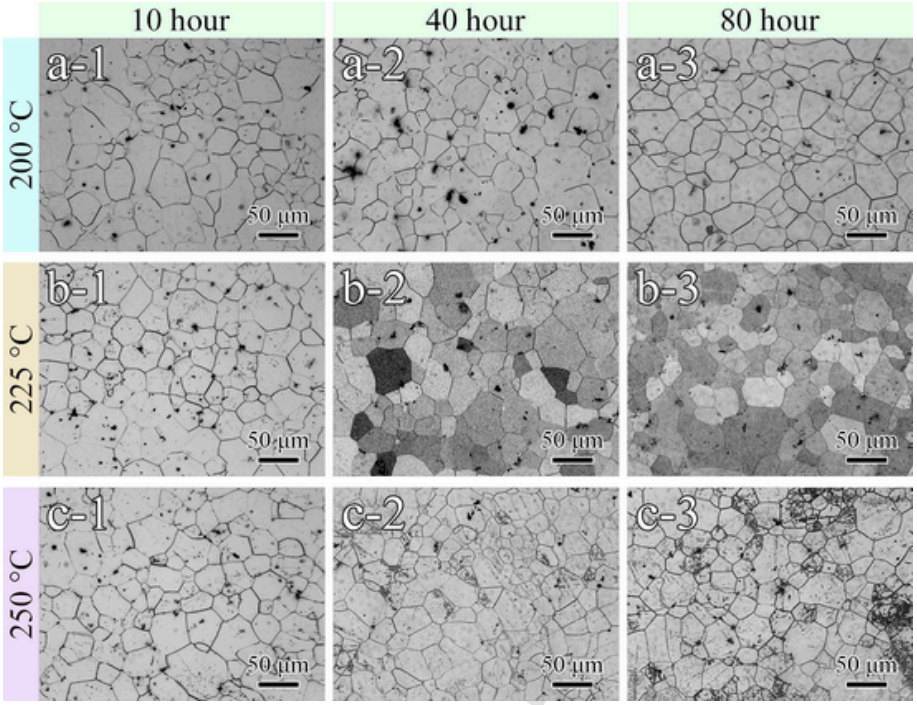

Fig. 4. Optical micrography of Mg—Gd alloy after aging treatment: (a-1) to (a-3) aged at 200 °C for 10 h, 40 h and 80 h, respectively; (b-1) to (b-3) aged at 225 °C for 10 h, 40 h and 80 h, respectively; (c-1) to (c-3) aged at 250 °C for 10 h, 40 h and 80 h, respectively.

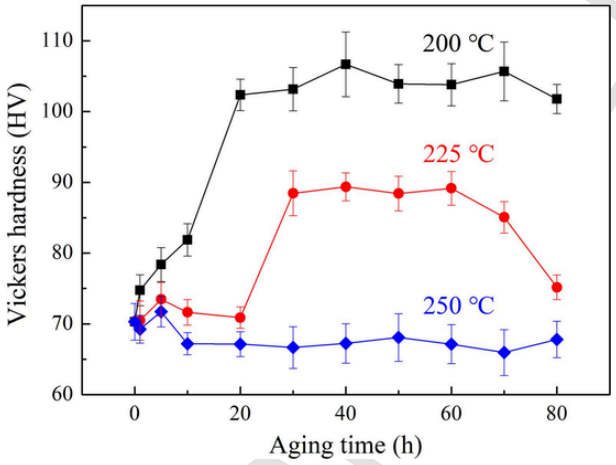

Fig. 5. Age-hardening curves of Mg—Gd samples treated at 200 °C, 225 °C and 250 °C, respectively.

3.2. Aging microstructures and hardening curves

Fig. 4 shows the metallographic structures of Mg—Gd samples after aging treatment at 200 °C, 225 °C and 250 °C from 10 h to 40 h and 80 h, respectively. Since the aging temperature is much lower than the recrystallization temperature (450 °C) of Mg—10Gd alloy, all the aged samples exhibit a close average grain size. As shown in Fig. 4a-1, a-2 and a-3, no significant difference is found in the microstructure contrast of three samples, which annealed at 200 °C for 10, 40 and 80 h, respectively. As the temperature increases to 225 °C, the image contrast of the samples aged for 40 and 80 h (Fig. 4b-2 and b-3) exhibits much different from that of aged for 10 h (Fig. 4b-1), which is mainly due to the formation of nano-precipitates in the samples. As the aging temperature increases to 250 °C, some floccules composed of coarse precipitates are observed in the samples treated for 40 h and 80 h (Fig. 4c-2 and c-3).

Fig. 5 shows the age hardening curves of Mg—Gd samples treated at three temperatures of 200 °C, 225 °C and 250 °C for 5–80 h. It is clearly that the annealed sample exhibits an improvement of microhardness from 70.3 HV to 102.4 HV after aging at 200 °C for 20 h. Then, the hardness of the samples keeps stable during the next 20 h at 200 °C. The aging time for reaching the peak stage (88.5 HV) at 225 °C is 30 h, and the hardness decreases to 75.2 HV after aging for 80 h. In a sharp contrast, the hardness values of the samples have little change during 80 h of aging treatment, which indicates no hardening effect at 250 °C. Thus, the optimum aging temperature for Mg—Gd alloy is 200 °C, and it exhibits a certain aging hardening effect at 225 °C. Since the average grain sizes of the aged samples are not changed, the microhardness enhancement is induced by precipitation strengthening. Distinct hardening effects are obtained in the Mg—Gd samples treated by different aging processes, and the essential reason is that significant differences are found in the density and morphology of precipitates in each aged sample, which are needed to be further characterized and analyzed by TEM.

3.3. Precipitates evolution

Fig. 6 shows the HAADF-STEM images of Mg—Gd samples under different aging time at 200 °C. In the initial stage (aging for 5 h), the decomposition rate of supersaturated solid solutions in the sample is accelerated, and some solute Gd-rich regions are observed as well as initial nucleated precipitates, as shown in Fig. 6a. The petal-like β" phases, ordered GP zones and local disordered Gd-rich clusters are formed in this stage. Owing to the weak resistance of these small phases to dislocation slipping, the microhardness of Mg—Gd sample only shows a slight increasing. In order to reduce the local energy concentration, Gd atoms of the initial nucleated β" phases are orderly arranged, and the projections of these smallest β" cells on the (0001) plane present regular hexagons with twice the size of magnesium matrix. The β" phase exhibits the $D0_{19}$ superlattice structure with lattice constants of $a = 0.64$ nm and $c = 0.52$ nm, and its orientation relationships with the Mg matrix are $[0001]_{\beta''}//[0001]_{\alpha}$ and $(2\bar{1}\bar{1}0)_{\beta''}//(2\bar{1}\bar{1}0)_{\alpha}$. The habit

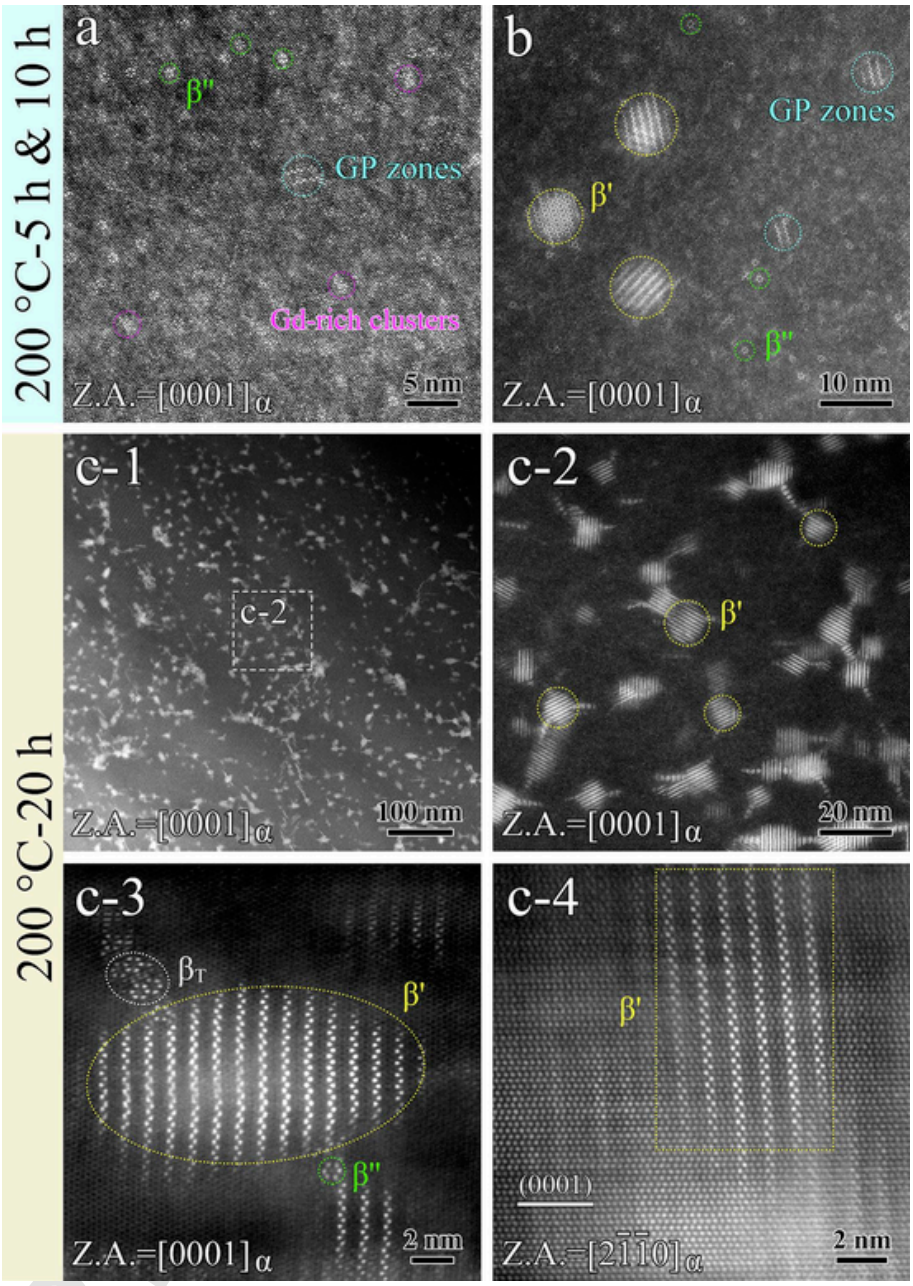

Fig. 6. HAADF-STEM images of Mg—Gd samples under different aging time at 200 °C: (a) aging time of 5 h; (b) aging time of 10 h; (c-1) aging time of 20 h; (c-2) local enlarged image of (c-1); (c-3) and (c-4) morphology of β' precipitate at the $[0001]_\alpha$ and $[2\bar{1}\bar{1}0]_\alpha$ zone axis, respectively.

plane of β" phase is $\{2\bar{1}\bar{1}0\}_\alpha$, and its chemical composition is Mg_3Gd [30–32].

As the aging time increases to 10 h, some new phases with ordered zigzag structures are formed in the matrix, which are determined as β' phases marked by yellow circles in Fig. 6b. The density of β' phases is relatively low with a size of ~10 nm. Besides β' phases, the initial petal-like β" phases and GP zones are still observed in the Mg matrix, which further indicates that the aging precipitation process of Mg—10Gd alloy is a dynamic and continuous process, in which the nucleation, phase transformation and growth behavior occur simultaneously. Apps et al. [33] pointed out that the β" phase plays a role of nucleation site in the formation of β' phase, and the Gd atoms of β" phase are reordered and evolved into β' phase. Compared with the annealed sample, the microhardness of this sample aged for 10 h is improved to 81.9 HV.

When the aging time further increases to 20 h, as shown in Fig. 6c-1 and c-2 at the $[0001]_\alpha$ zone axis, numerous nano-sized β' strengthening phases with zigzag structures are observed in the sample. Compared with the sample aged for 10 h, the size and density of these β' phases increase significantly, resulting in the hardness remarkably improved to 102.4 HV. Fig. 6c-3 shows that some antennular-shaped structures composed of β" and β_T phases are formed at the edge of β' precipitates. The β_T phases are also named tail-like structures raised by Zhang et al. [26]. The β" and β_T phases exhibit a lower nucleation barrier, and β' phases are connected by above two metastable phases to reduce the elastic strain and achieve growth [34]. Furthermore, the antennular-shaped structures continue to transform to β' phases during aging treatment. Fig. 6c-4 shows the morphology of β' precipitate observed from the $[2\bar{1}\bar{1}0]_\alpha$ zone axis, and its length along the $<01\bar{1}0>$ direction is ~6 nm. Compared with the basal precipitate plates and prismatic rods, β' precipitates provide a stronger blocking effect on basal dislocation slipping, leading to a better precipitation strengthening effect [7,10].

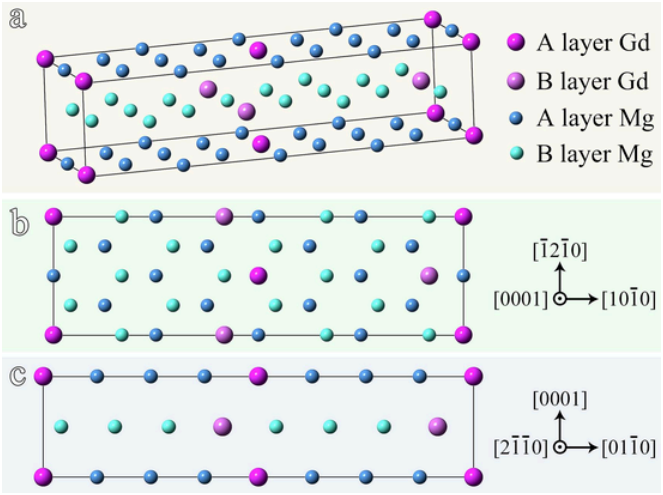

Fig. 7. Atomic model of β' precipitate: (a) 3D model; (b) [0001] zone axis; (c) [$2\bar{1}\bar{1}0$] zone axis.

The nano-scaled β' precipitates are the main strengthening phases in the peak aging stage at 200 °C. Based on the atomic morphologies observed from $[0001]_\alpha$ and $[2\bar{1}\bar{1}0]_\alpha$ directions (see Fig. 6c-3 and c-4), the atomic model of crystal structure for β' precipitate is established, as shown in Fig. 7. The β' phase exhibits a *c*-axis base-centered orthogonal (cbco) structure distributed coherent with the Mg matrix, and its formation mainly origins from Mg atoms substituted by Gd atoms in the lattice. The lattice constants of β' phase are $a = 0.642$ nm, $b = 2.224$ nm and $c = 0.52$ nm, and its orientation relationships with the Mg matrix are $[001]_{\beta'}//[0001]_\alpha$ and $(100)_{\beta'}//(2\bar{1}\bar{1}0)_\alpha$. The habit plane of β' phase is $\{2\bar{1}\bar{1}0\}_\alpha$, and its chemical composition is Mg_7Gd [35,36].

When the aging temperature increases to 225 °C, as shown in Fig. 8a, the morphology of precipitates changes significantly, showing the gourd-shaped structures with average long-axis size of ~100 nm. The microhardness of the sample aged for 40 h is improved to 89.4 HV, but the strengthening effect is inferior to that of the samples aged at 200 °C. Furthermore, the high resolution HAADF-STEM image (Fig. 8b) shows that the main body of the gourd-shaped precipitates are still β' phases, and two different metastable phases (β_M and β_F') are observed in the connection region between β' phases. The characteristics of β_M phase is that Gd atoms are arranged in the form of continuous regular hexagons, and β_F' phase is characterized by the zigzag-arranged Gd atoms containing the same orientation relationship. Both β_M and β_F' phases are also considered to be the intermediate phases appeared in the process of β' phases transforming into incoherent β_1 phases [25,26]. When the aging time further prolongs to 80 h, the chain-like structure formed by the aggregation of precipitates appears in the sample, as shown in Fig. 8c. Meanwhile, the dispersed β' phases grow up and coarsen gradually, eventually forming β_1 phases marked by purple arrows in Fig. 8d. These two types of phases (β' and β_1) coexist in this sample, but the strengthening effect becomes lower, resulting in the microhardness down to 75.2 HV.

At present, a reasonable explanation for the nucleation mechanism of β_1 phase is that at the necking position of β' phase under decomposition state, β_1 phase is nucleated and subsequently coarsened by consuming β' phase with the diffusion of solute Gd atoms [26]. The β_1 phase exhibits the face-centered cubic (FCC) structure with lattice constant of $a = 0.73$ nm, and its orientation relationships with the Mg matrix are $[001]_{\beta1}//[0001]_\alpha$ and $(1\bar{1}2)_{\beta1}//(10\bar{1}0)_\alpha$. The habit plane of β_1 phase is $\{10\bar{1}0\}_\alpha$, and its chemical composition is Mg_3Gd [37]. The β_1

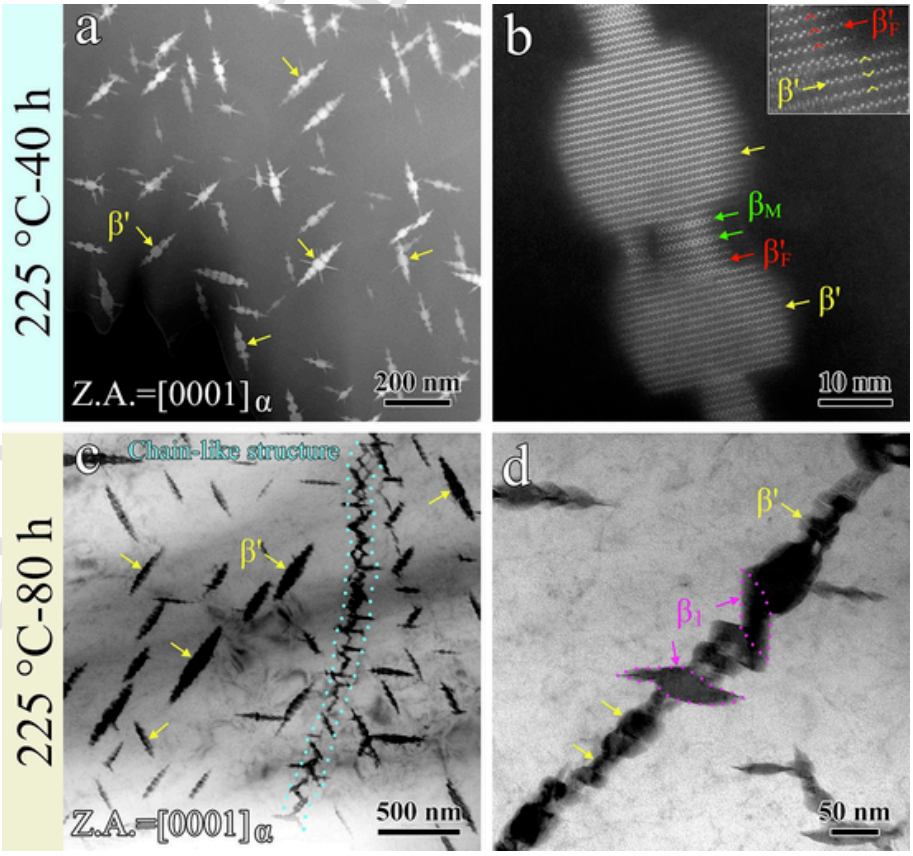

Fig. 8. Precipitate morphology of Mg—Gd samples under different aging time at 225 °C: (a) and (b) HAADF-STEM images under aging time of 40 h; (c) and (d) TEM images under aging time of 80 h.

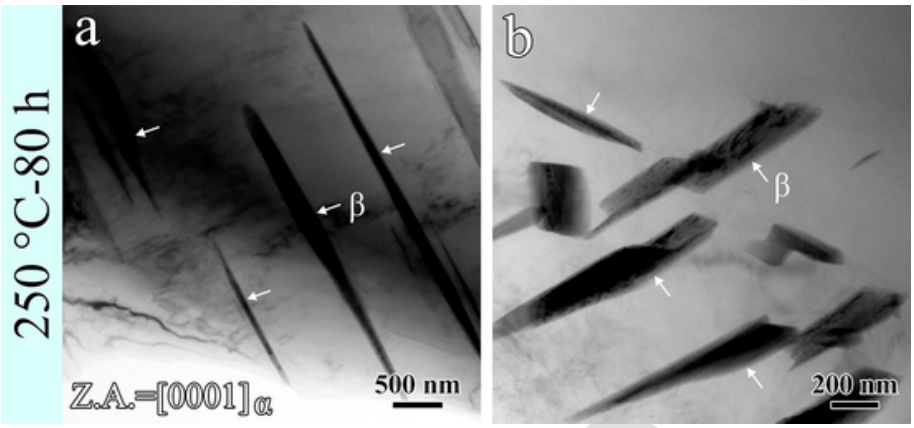

Fig. 9. TEM images of Mg—Gd sample aged at 250 ˚C for 80 h: (a) rod-shaped β precipitates; (b) square-shaped β precipitates.

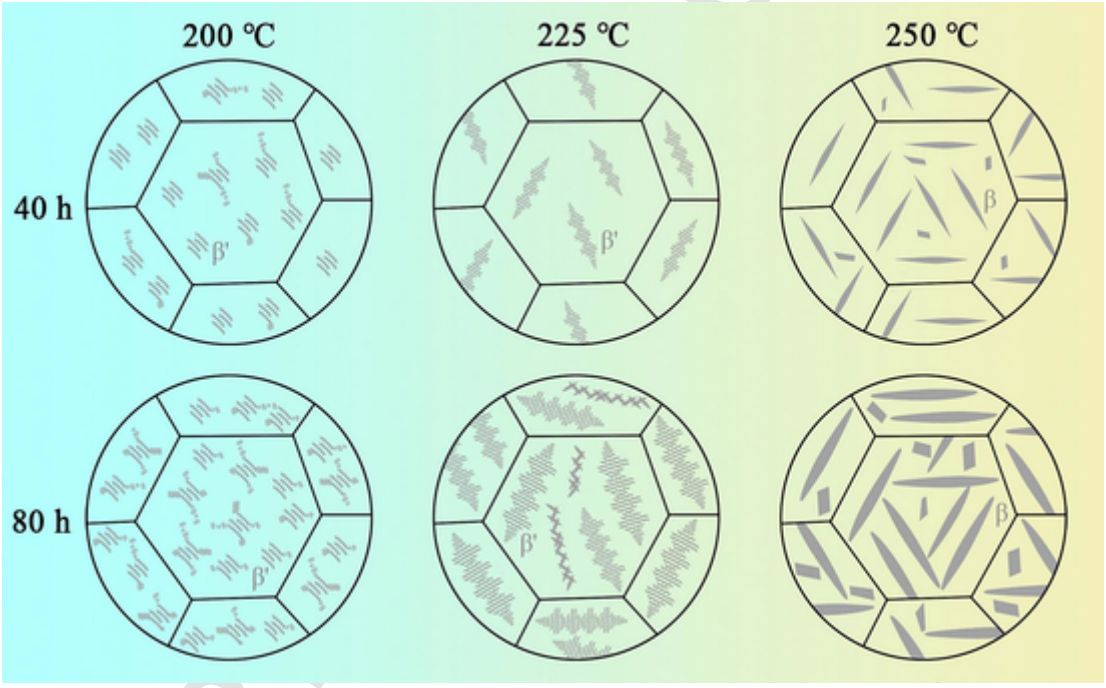

Fig. 10. Schematic illustration of the precipitation evolutions of Mg—10Gd alloy under different aging process.

phase is coherent with the Mg matrix on the habit plane, but the interfaces formed at the top and bottom planes perpendicular to the habit plane are semi-coherent [34].

Fig. 9 shows the morphology of precipitates in Mg—Gd sample aged at 250 ˚C for 80 h. Numerous rod-shaped β phases marked by white arrows in Fig. 9a are formed in the matrix, as well as square-shaped β phases with average long-axis size of ~600 nm (Fig. 9b). The lattice constant of equilibrium β phase is $a = 2.23$ nm, and its orientation relationships with the Mg matrix are $[110]_{\beta}//[0001]_{\alpha}$ and $(\bar{1}12)_{\beta}//(1\bar{1}00)_{\alpha}$ [37].

From the perspective of aging precipitation kinetics of Mg—10Gd alloy, the rapid diffusion rate of solute Gd atoms facilitates the dynamic precipitation of β' nano-phases, and the time required to reach the peak aging stage is short, resulting in the optimum hardening effect in the samples aged at 200 ˚C. When aging temperature exceeds the suitable range, the whole precipitation process occurs quite rapidly, and the solute supersaturation in Mg matrix decreases quickly after reaching the peak stage, which causing the reduction of driving forces for solid solution decomposition [38]. The β' precipitates grow up and coarsen gradually or evolve into other phases (such as β_1 and β), which leading to the undesirable strengthening effect in the samples treated at over 225 ˚C.

Above all, the stages of microstructural changes and precipitation evolutions of Mg—10Gd alloy treated by different aging process are schematically illustrated in Fig. 10. Similar grain structures are observed in Mg—10Gd alloy after different aging treatment, but diverse precipitate morphologies are formed in the matrix. β' nano-precipitates are visible in the peak aging stage at 200 ˚C for over 20 h. With increasing aging temperature to 225 ˚C, gourd-shaped β' precipitates become the dominating strengthening phases, and β' phases grow up and coarsen gradually with the prolong of aging time. The highest aging temperature of 250 ˚C results in the continuing occurrence of phase transformations, leading to coarse rod-shaped and square-shaped β phases formed in the samples aged for over 40 h.

4. Conclusions

In summary, the aging hardening characteristic and precipitate evolution of Mg—10Gd alloy at different temperatures were systemati-

cally investigated by characterizing methods including OM, EBSD, TEM and HAADF-STEM. The key findings are summarized as follows:

(1) The optimum aging temperature of Mg—10Gd alloy is 200 °C, and the peak hardness reaches up to 102.4 HV. The aging hardening effect is weakened at 225 °C and vanished at 250 °C.

(2) The average grain sizes are stable during aging. The microhardness improvements mainly result from precipitation hardening. β' nano-precipitates with fine size of ~10 nm are the main strengthening phases. The strengthening effect of the aged samples at 225 °C decreases with peak hardness of 89.4 HV, which is mainly due to the coarse gourd-shaped β' precipitates with a size of ~100 nm.

(3) The aging treatment of Mg—10Gd alloy is a dynamic and continuous process, in which various metastable structures (including short-range ordered GP zones, β'', β_T, β_M and β_F' phases) are observed in the aged samples.

Data availability statement

The raw/processed data required to reproduce these findings cannot be shared at this time as the data also forms part of an ongoing study.

CRediT authorship contribution statement

Kang Wei: Investigation, Data curation, Visualization, Writing-original draft. **Lirong Xiao:** Methodology, TEM, Formal analysis. **Bo Gao:** Investigation, TEM. **Qingzhong Mao:** Investigation, Data curation. **Yi Liu:** Visualization, Formal analysis. **Lei Li:** Investigation, Validation. **Wenwen Sun:** TEM, Data curation. **Yudong Sui:** Methodology, Investigation. **Hao Zhou:** Conceptualization, Writing-review & editing, Formal analysis, Funding acquisition. **Yonghao Zhao:** Conceptualization, Supervision, Writing-review & editing, Funding acquisition.

Declaration of Competing Interest

The authors declare that they have no known competing financial interests or personal relationships that could have appeared to influence the work reported in this paper.

Data availability

Data will be made available on request.

Acknowledgments

This work was supported by the National Key Research and Development Program of China (grant number 2021YFA1200203), the Key Program of National Natural Science Foundation of China (grant number 51931003), the National Natural Science Foundation of China (grant numbers 52071178, 52171118, 51901103, 51971112), the Fundamental Research Funds for the Central Universities (grant number 30918011342), the Natural Science Foundation for Young Scholars of Jiangsu Province (grant number BK20200387) and Jiangsu Funding Program for Excellent Postdoctoral Talent (grant number 2022ZB279). The authors wish to express their appreciation to the Jiangsu Key Laboratory of Advanced Micro&Nano Materials and Technology. EBSD and TEM experiments were performed at Center of Analytical Facilities of Nanjing University of Science and Technology.

References

[1] T.M. Pollock, Weight loss with magnesium alloys, Science 328 (2010) 986–987.
[2] B.C. Suh, M.S. Shim, K.S. Shin, N.J. Kim, Current issues in magnesium sheet alloys: where do we go from here? Scr. Mater. 84–85 (2014) 1–6.
[3] K. Wei, R. Hu, D.D. Yin, L.R. Xiao, S. Pang, Y. Cao, H. Zhou, Y.H. Zhao, Y.T. Zhu, Grain size effect on tensile properties and slip systems of pure magnesium, Acta Mater. 206 (2021) 116604.
[4] J.W. Lu, D.D. Yin, G.H. Huang, G.F. Quan, Y. Zeng, H. Zhou, Q.D. Wang, Plastic anisotropy and deformation behavior of extruded mg-Y sheets at elevated temperatures, Mater. Sci. Eng. A 700 (2017) 598–608.
[5] L.R. Xiao, Y. Cao, S. Li, H. Zhou, X.L. Ma, L. Mao, X.C. Sha, Q.D. Wang, Y.T. Zhu, X.D. Han, The formation mechanism of a novel interfacial phase with high thermal stability in a mg-Gd-Y-ag-Zr alloy, Acta Mater. 162 (2019) 214–225.
[6] K. Wei, L.R. Xiao, B. Gao, L. Li, Y. Liu, Z.G. Ding, W. Liu, H. Zhou, Y.H. Zhao, Enhancing the strain hardening and ductility of mg-Y alloy by introducing stacking faults, J. Magn. Alloys 8 (2020) 1221–1227.
[7] J.F. Nie, Precipitation and hardening in magnesium alloys, Metall. Mater. Trans. A 43 (2012) 3891–3939.
[8] J. Jain, P. Cizek, W.J. Poole, M.R. Barnett, Precipitate characteristics and their effect on the prismatic-slip-dominated deformation behaviour of an mg-6Zn alloy, Acta Mater. 61 (2013) 4091–4102.
[9] J.H. Zhang, S.J. Liu, R.Z. Wu, L.G. Hou, M.L. Zhang, Recent developments in high-strength mg-RE-based alloys: focusing on mg-Gd and mg-Y systems, J. Magn. Alloys 6 (2018) 277–291.
[10] J.F. Nie, Effects of precipitate shape and orientation on dispersion strengthening in magnesium alloys, Scr. Mater. 48 (2003) 1009–1015.
[11] B.Y. Liu, N. Yang, J. Wang, M. Barnett, Y.C. Xin, D. Wu, R.L. Xin, B. Li, R.L. Narayan, J.F. Nie, J. Li, E. Ma, Z.W. Shan, Insight from in situ microscopy into which precipitate morphology can enable high strength in magnesium alloys, J. Mater. Sci. Technol. 34 (2018) 1061–1066.
[12] H.B. Xie, H.C. Pan, Y.P. Ren, S.N. Sun, L.Q. Wang, Y.F. He, G.W. Qin, Co-existences of the two types of β' precipitations in peak-aged mg-Gd binary alloy, J. Alloys Compd. 738 (2018) 32–36.
[13] D. Choudhuri, S.G. Srinivasan, Density functional theory-based investigations of solute kinetics and precipitate formation in binary magnesium-rare earth alloys: a review, Comput. Mater. Sci. 159 (2019) 235–256.
[14] R.G. Li, J.F. Nie, G.J. Huang, Y.C. Xin, Q. Liu, Development of high-strength magnesium alloys via combined processes of extrusion, rolling and ageing, Scr. Mater. 64 (2011) 950–953.
[15] J. Čížek, I. Procházka, B. Smola, I. Stulíková, V. Očenášek, Influence of deformation on precipitation process in mg-15wt.%Gd alloy, J. Alloys Compd. 430 (2007) 92–96.
[16] Y.C. Wan, B. Tang, Y.H. Gao, L.L. Tang, G. Sha, B. Zhang, N.N. Liang, C.M. Liu, S.N. Jiang, Z.Y. Chen, X.Y. Guo, Y.H. Zhao, Bulk nanocrystalline high-strength magnesium alloys prepared via rotary swaging, Acta Mater. 200 (2020) 274–286.
[17] R.G. Li, H.B. Shafqat, J.H. Zhang, R.Z. Wu, G.Y. Fu, L. Zong, Y. Su, Cold-working mediated converse age hardening responses in extruded mg-14Gd-2Ag-0.5Zr alloy with different microstructure, Mater. Sci. Eng. A 748 (2019) 95–99.
[18] A. Issa, J.E. Saal, C. Wolverton, Formation of high-strength β' precipitates in mg-RE alloys: the role of mg/β interfacial instability, Acta Mater. 83 (2015) 75–83.
[19] Y.Z. Ji, A. Issa, T.W. Heo, J.E. Saal, C. Wolverton, L.Q. Chen, Predicting β' precipitate morphology and evolution in mg-RE alloys using a combination of first-principles calculations and phase-field modeling, Acta Mater. 76 (2014) 259–271.
[20] L.L. Rokhlin, Magnesium Alloys Containing Rare Earth Metals: Structure and Properties, Taylor & Francis, London, 2003, pp. 97–99.
[21] S.Q. Liang, D.K. Guan, X.P. Tan, L. Chen, Y. Tang, Effect of isothermal aging on the microstructure and properties of as-cast mg-Gd-Y-Zr alloy, Mater. Sci. Eng. A 528 (2011) 1589–1595.
[22] C. Xu, M.Y. Zheng, K. Wu, E.D. Wang, G.H. Fan, S.W. Xu, S. Kamado, X.D. Liu, G.J. Wang, X.Y. Lv, Effect of ageing treatment on the precipitation behaviour of mg-Gd-Y-Zn-Zr alloy, J. Alloys Compd. 550 (2013) 50–56.
[23] S.M. He, X.Q. Zeng, L.M. Peng, X. Gao, J.F. Nie, W.J. Ding, Microstructure and strengthening mechanism of high strength mg-10Gd-2Y-0.5Zr alloy, J. Alloys Compd. 427 (2007) 316–323.
[24] H. Zhou, W.Z. Xu, W.W. Jian, G.M. Cheng, X.L. Ma, W. Guo, S.N. Mathaudhu, Q.D. Wang, Y.T. Zhu, A new metastable precipitate phase in mg-Gd-Y-Zr alloy, Philos. Mag. 94 (2014) 2403–2409.
[25] J.K. Zheng, R.C. Luo, X.Q. Zeng, B. Chen, Nano-scale precipitation and phase growth in mg-Gd binary alloy: an atomic-scale investigation using HAADF-STEM, Mater. Des. 137 (2018) 316–324.
[26] Y. Zhang, W. Rong, Y.J. Wu, L.M. Peng, J.F. Nie, N. Birbilis, A detailed HAADF-STEM study of precipitate evolution in mg-Gd alloy, J. Alloys Compd. 777 (2019) 531–543.
[27] Z. Xu, M. Weyland, J.F. Nie, On the strain accommodation of β_1 precipitates in magnesium alloy WE54, Acta Mater. 75 (2014) 122–133.
[28] J.X. Zheng, Z. Li, L.D. Tan, X.S. Xu, R.C. Luo, B. Chen, Precipitation in mg-Gd-Y-Zr alloy: atomic-scale insights into structures and transformations, Mater. Charact. 117 (2016) 76–83.
[29] H. Zhou, Q.D. Wang, J. Chen, B. Ye, W. Guo, Microstructure and Mechanical Properties of Extruded mg-8.5Gd-2.3Y-1.8Ag-0.4Zr Alloy, Trans. Nonferrous Met. Soc. China, vol. 22, 2012, pp. 1891–1895.
[30] C. Antion, P. Donnadieu, F. Perrard, A. Deschamps, C. Tassin, A. Pisch, Hardening precipitation in a mg-4Y-3RE alloy, Acta Mater. 51 (2003) 5335–5348.
[31] T. Honma, T. Ohkubo, K. Hono, S. Kamado, Chemistry of nanoscale precipitates in mg-2.1Gd-0.6Y-0.2Zr(at.%) alloy investigated by the atom probe technique, Mater. Sci. Eng. A 395 (2005) 301–306.
[32] L. Zhang, M. Gong, L.M. Peng, Microstructure and strengthening mechanism of a thermomechanically treated mg-10Gd-3Y-1Sn-0.5Zr alloy, Mater. Sci. Eng. A 565 (2013) 262–268.
[33] P.J. Apps, H. Karimzadeh, J.F. King, G.W. Lorimer, Precipitation reactions in magnesium-rare earth alloys containing yttrium, gadolinium or dysprosium, Scr. Mater. 48 (2003) 1023–1028.
[34] S.M. He, X.Q. Zeng, L.M. Peng, X. Gao, J.F. Nie, W.J. Ding, Precipitation in a mg-10Gd-3Y-0.4Zr (wt.%) alloy during isothermal ageing at 250°C, J. Alloys Compd.

421 (2006) 309–313.
[35] M. Nishijima, K. Hiraga, M. Yamasaki, Y. Kawamura, Characterization of β' phase precipitates in an mg-5at%Gd alloy aged in a peak hardness condition, studied by high-angle annular detector dark-field scanning transmission electron microscopy, Mater. Trans. 47 (2006) 2109–2112.
[36] M. Nishijima, K. Hiraga, Structural changes of precipitates in an mg-5at%Gd alloy studied by transmission electron microscopy, Mater. Trans. 48 (2007) 10–15.
[37] J.F. Nie, B.C. Muddle, Characterisation of strengthening precipitate phases in a mg-Y-Nd alloy, Acta Mater. 48 (2000) 1691–1703.
[38] L.L. Rokhlin, Magnesium Alloys Containing Rare Earth Metals: Structure and Properties, Taylor & Francis, 2003, pp. 97–99.